Fibroblast-specific inhibition of TGF-β1 signaling attenuates lung and tumor fibrosis

Ying Wei,[1] Thomas J. Kim,[1] David H. Peng,[2] Dana Duan,[3] Don L. Gibbons,[2] Mitsuo Yamauchi,[4] Julia R. Jackson,[1] Claude J. Le Saux,[1,5] Cheresa Calhoun,[5] Jay Peters,[5] Rik Derynck,[3] Bradley J. Backes,[1] and Harold A. Chapman[1]

[1]Department of Medicine, UCSF Cardiovascular Research Institute, San Francisco, California, USA. [2]Departments of Thoracic/Head and Neck Medical Oncology and Molecular and Cellular Oncology, The University of Texas MD Anderson Cancer Center, Houston, Texas, USA. [3]Department of Cell and Tissue Biology, UCSF, San Francisco, California, USA. [4]Oral and Craniofacial Health Sciences, University of North Carolina at Chapel Hill, Chapel Hill, North Carolina, USA. [5]Department of Pulmonary and Critical Care, University of Texas Health Science Center at San Antonio, San Antonio, Texas, USA.

TGF-β1 signaling is a critical driver of collagen accumulation and fibrotic disease but also a vital suppressor of inflammation and epithelial cell proliferation. The nature of this multifunctional cytokine has limited the development of global TGF-β1 signaling inhibitors as therapeutic agents. We conducted phenotypic screens for small molecules that inhibit TGF-β1–induced epithelial-mesenchymal transition without immediate TGF-β1 receptor (TβR) kinase inhibition. We identified trihydroxyphenolic compounds as potent blockers of TGF-β1 responses (IC_{50} ~50 nM), Snail1 expression, and collagen deposition in vivo in models of pulmonary fibrosis and collagen-dependent lung cancer metastasis. Remarkably, the functional effects of trihydroxyphenolics required the presence of active lysyl oxidase–like 2 (LOXL2), thereby limiting effects to fibroblasts or cancer cells, the major LOXL2 producers. Mechanistic studies revealed that trihydroxyphenolics induce auto-oxidation of a LOXL2/3–specific lysine (K731) in a time-dependent reaction that irreversibly inhibits LOXL2 and converts the trihydrophenolic to a previously undescribed metabolite that directly inhibits TβRI kinase. Combined inhibition of LOXL2 and TβRI activities by trihydrophenolics resulted in potent blockade of pathological collagen accumulation in vivo without the toxicities associated with global inhibitors. These findings elucidate a therapeutic approach to attenuate fibrosis and the disease-promoting effects of tissue stiffness by specifically targeting TβRI kinase in LOXL2-expressing cells.

Introduction

Tissue fibrosis is a major cause of human morbidity and mortality worldwide (1, 2). TGF-β1 signaling through its heterotetrameric receptor complex of 2 receptor types, TβRII and TβRI, is a well-known driver of collagen expression and tissue accumulation important to wound repair (3). Exaggerated TGF-β1 signaling is also strongly implicated in numerous fibrotic diseases, including those involving liver, heart, and lung (4–7). For example, approximately 80% of the upregulated genes in lungs of patients with idiopathic pulmonary fibrosis are reported to be direct or indirect TGF-β1 target genes (8). Pathological collagen accumulation, and its promoting effects on tissue stiffness, are also strongly implicated in cancer progression (9–11). TGF-β1 signaling is both an initiator and a driver of tissue stiffness because accumulation of collagen and other matrix proteins promotes integrin-dependent latent TGF-β1 activation and further extracellular matrix deposition (12). Enhanced stiffness is thought to promote tumor cell β_1 integrin activation, leading to more invasive tumor phenotypes and metastasis, consistent with the strong correlation of TGF-β1 signaling with poor cancer prognosis (9, 13, 14). For these and other reasons there has been much interest in TGF-β1 signaling as a therapeutic target (15–17).

Although attractive as a target, the critical roles of TGF-β1 in suppressing inflammation and epithelial proliferation give pause to the idea of global inhibition of TGF-β1 signaling (18). Indeed, systemic inhibition of TGF-β1 can lead to the development of squamous skin tumors and autoreactive immunity (18–21). In addition, chronic administration of several small-molecule inhibitors of TGF-β1 receptor (TβR) kinases has led to enhanced skin and colonic inflammation and abnormalities in cardiac valves (22, 23). To minimize adverse consequences, an approach of blocking TGF-β1 activation in specific cell types using the unique pathway of $\alpha_v\beta_6$-dependent latent TGF-β1 activation has developed and is currently in clinical trial (24). But this integrin is primarily expressed in epithelia of lung, kidney, and skin (25). In an attempt to develop a more circumscribed inhibitor of TGF-β1 signaling centered on suppression of collagen accumulation, we undertook a high-throughput, image-based phenotypic screen of small molecules that could block TGF-β1–induced epithelial-mesenchymal transition (EMT) in vitro but not directly inhibit TβRI kinase itself. We identified compounds of the ellagitannin and catechin families that met these criteria and then explored the underlying mechanisms, ultimately revealing a novel approach to fibroblast-selective inhibition of TGF-β1 signaling.

Results

Phenotypic screen identifies small molecules with antifibrotic activity in vivo. We took advantage of the dramatic phenotypic switch in A549 lung adenocarcinoma cells upon TGF-β1 stimulation resulting in

Conflict of interest: The authors have declared that no conflict of interest exists.
Submitted: April 18, 2017; **Accepted:** July 18, 2017.
Reference information: *J Clin Invest*. 2017;127(10):3675–3688.
https://doi.org/10.1172/JCI94624.

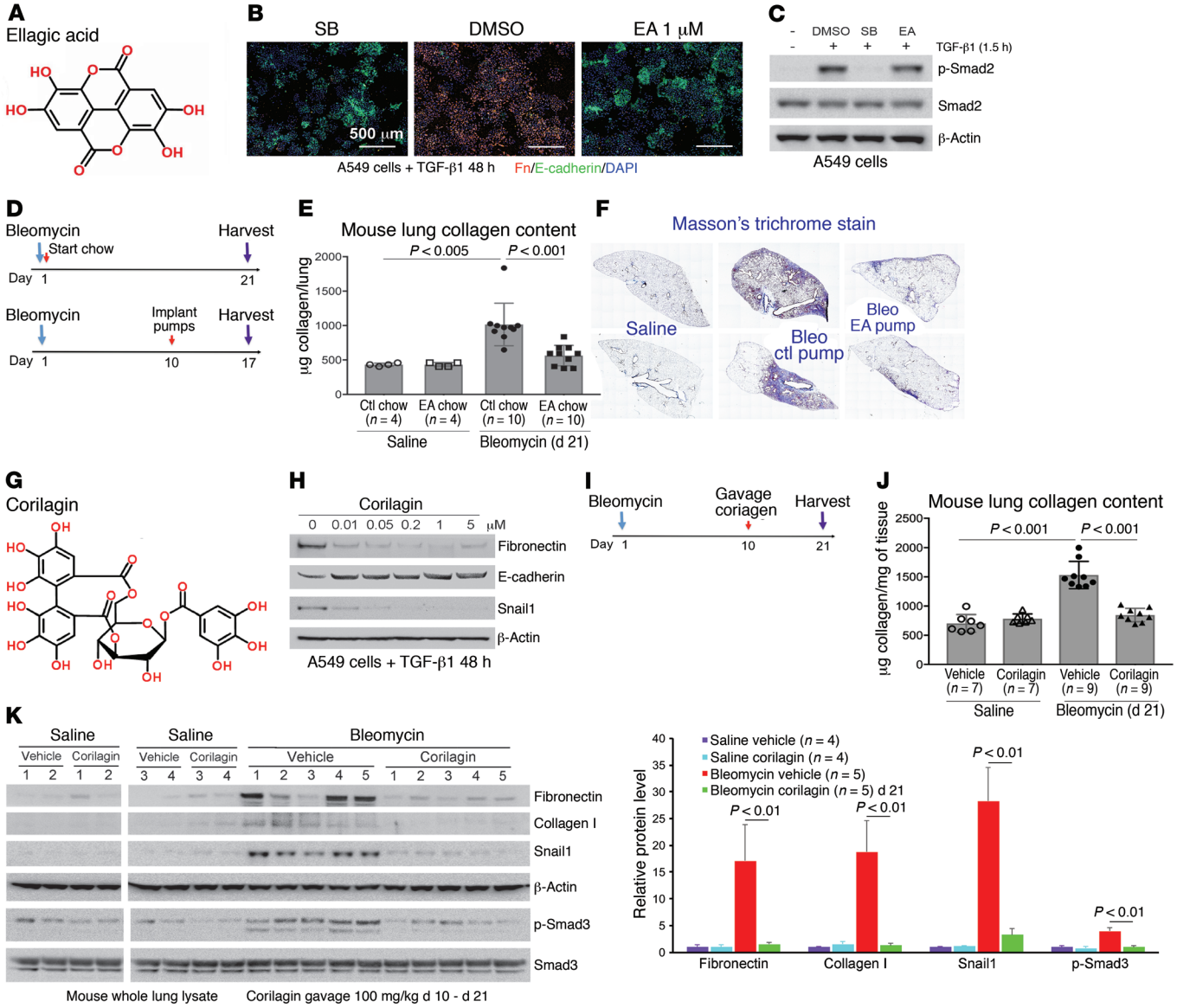

Figure 1. EA and corilagin inhibit TGF-β1–dependent EMT and attenuate bleomycin-induced fibrogenesis. (**A**) Structure of EA. (**B**) Immunofluorescence of TGF-β1–stimulated A549 cells treated with DMSO, SB431542 (SB), or EA. Green, E-cadherin; orange, fibronectin; blue, DAPI. Scale bars: 500 μm. Each assay was performed in triplicate. (**C**) A549 cells were treated with EA (1 μM) and TGF-β1 for 1.5 hours and lysates immunoblotted for p-Smad2, Smad2, and β-actin. Repeat = 3. (**D**) EA dosing and treatment in lung fibrosis model. EA and control (ctl) chow were given to mice for 21 days. Osmotic pumps with EA or PBS were implanted on mice for 7 days at day 10 after bleomycin. (**E**) Hydroxyproline analysis of lung tissues from mice given saline ctl chow ($n = 4$), saline EA chow ($n = 4$), bleomycin ctl chow ($n = 10$), and bleomycin EA chow ($n = 10$). Data represent mean ± SD. (**F**) Masson's trichrome staining of lung sections from ctl or EA pump–treated mice 17 days after bleomycin. Mosaic images (×4) covering whole lung section are shown. (**G**) Structure of corilagin. (**H**) A549 cells stimulated with TGF-β1 were treated with corilagin (0–5 μM) for 48 hours and lysates blotted for fibronectin, E-cadherin, Snail1, and β-actin. Repeat = 3. (**I**) Corilagin dosing and treatment in lung fibrosis model. Vehicle or corilagin was given to mice by daily gavage starting from day 10 after bleomycin for 11 days. (**J**) Hydroxyproline analysis of lung tissues from mice treated with saline vehicle ($n = 7$), saline corilagin ($n = 7$), bleomycin vehicle ($n = 9$), and bleomycin corilagin ($n = 9$). Data represent mean ± SD. (**K**) Whole lung lysates from mice given saline vehicle ($n = 4$), saline corilagin ($n = 4$), bleomycin vehicle ($n = 5$), and bleomycin corilagin ($n = 5$) were blotted for fibronectin, collagen I, Snail1, β-actin, p-Smad3, and total Smad3. Quantification of bands normalized to β-actin is expressed as mean ± SD. Data in **E**, **J**, and **K** were analyzed by 1-way ANOVA with a Tukey post hoc test.

loss of E-cadherin expression and induction of fibronectin (26). Several small-molecule libraries totaling approximately 40,000 compounds composed of both diverse and bioactive compounds were screened. We identified ellagic acid (EA) as one compound meeting our criteria (Figure 1, A–C, and Supplemental Figure 1A; supplemental material available online with this article; https://doi.org/10.1172/JCI94624DS1). We next examined the structural determinants of TGF-β1–induced EMT suppression in A549 cells by other polyphenol family members and found that only polyphenols with at least 1 trihydroxyphenolic motif in their primary structure inhibited Snail1 expression and their potency of inhibition correlated with the number of trihydroxyphenolic units (Supplemental Figure 1, B–D). This point is best illustrated by a comparison of epicatechin (EC) and epigallocatechin (EGC), which are struc-

turally identical aside from a dihydroxy- rather than the trihydroxyphenolic motif in EC (Supplemental Figure 1C). EC had no activity in our in vitro assays, whereas EGC was a potent inhibitor of Snail1 and fibronectin in TGF-β1–stimulated A549 cells.

EA was then tested for its antifibrotic activity in vivo by either ad libitum feeding of chow composed of 2% wt/wt raspberry extract rich in EA and EA precursors given to mice or administration of EA using osmotic pump (days 10–17) after intratracheal bleomycin (Figure 1D). We found that either treatment substantially improved survival (Table 1) and inhibited collagen accumulation (Figure 1, E and F). Because EA is poorly soluble, a more soluble trihydroxyphenolic-containing compound, corilagin, with an IC_{50} for EMT of approximately 50 nM (Figure 1, G and H), was given daily by gavage beginning 10 days after intratracheal bleomycin (Figure 1I). At day 21 these mice exhibited marked attenuation of bleomycin-induced total lung collagen, fibronectin, Snail1, and p-Smad3 (Figure 1, J and K). The average circulating level of corilagin 2 hours after the last dose was about 80 nM (Supplemental Figure 1E). EA-rich chow and corilagin had no effect on immune cell numbers or markers of injury (Supplemental Figure 2). Collectively, these findings demonstrate that trihydroxyphenolic compounds attenuate TGF-β1–induced Snail1 and EMT markers in vitro as well as collagen accumulation in vivo and do so at low nanomolar levels. Members of this polyphenol family have previously been shown to inhibit TGF-β1 signaling at micromolar levels in vitro and fibrosis in vivo but by unclear mechanisms (27, 28).

To test the efficacy of EA in a second in vivo model of tissue fibrosis, we examined the occurrence of metastatic lung nodules in mice injected subcutaneously 5 weeks earlier with syngeneic KrasG12D/p53R172H metastatic lung cancer cells (344SQ), known to metastasize as a function of the cross-linked fibrillar collagen content of the primary tumors (Figure 2A) (29). Consumption of EA-rich chow following tumor implantation markedly reduced the numbers of metastatic lung nodules (Figure 2, B and C). Although primary tumor volume or weight was unchanged (Figure 2, D and E), immunohistochemistry showed significantly reduced collagen I expression within the primary tumors treated with EA chow (Figure 2F). Furthermore, immunoblotting of these tumor extracts also revealed attenuated total fibronectin and collagen I expression, and decreased Smad activation, assessed by p-Smad3 (Figure 2G). Interestingly, visualizing collagen in situ by second-harmonics microscopy, we observed that the primary tumor collagen in mice fed EA chow was not only reduced but also exhibited more curved structures, suggesting less cross-linking (Figure 2, H and I, and ref. 9).

LOXL2 is identified as the target of trihydroxyphenolic-containing compounds. We next turned to underlying mechanisms that could account for the activities and potency of the polyphenolic compounds. Because of the striking inhibition of Snail1 expression by several trihydroxyphenolic compounds (Figure 1H and Supplemental Figure 1B), as well as the altered collagen cross-linking structure in primary 344SQ tumors (Figure 2I), we explored the hypothesis that lysyl oxidase–like 2 (LOXL2) was their target. LOXL2 has previously been linked to Snail1 accumulation in tumor cells (30), and its expression is potently induced by both hypoxia and TGF-β1 (31, 32). LOXL2, like all mammalian copper-dependent LOX enzymes, utilizes an intrinsically generated quinone, termed LTQ, to mediate oxidation of lysine primary amines (refs. 33, 34, and Figure 3A). The catalytic site quinone oxidizes the primary amines of collagen lysine (Lys) and hydroxylysine (Hyl) residues, releasing the respective aldehydes, Lys^{ald} and Hyl^{ald}, creating an intermediate aminophenol followed by release of H_2O_2 and NH_3, completing the LTQ cycle. Lys^{ald} and Hyl^{ald} in monomeric collagens then undergo a series of spontaneous condensation reactions that result in the formation of intra- and intermolecular covalent collagen cross-links (35).

Table 1. The survival of bleomycin-treated mice by day 21 of EA chow and day 17 of EA pump treatment

		EA	Control	χ^2 Test
Chow	Alive	10	6	$P = 0.0308$
	Dead	4	8	
Pump	Alive	10	6	$P = 0.0154$
	Dead	1	5	
Total	Alive	20	12	$P = 0.0014$
	Dead	5	13	

We first established an assay of collagen cross-linking induced by recombinant LOXL2 (36, 37) and found that corilagin and all other trihydroxyphenolics tested prevented cross-linking ($IC_{50} = 10$ nM; Supplemental Figure 3, A–C) whereas an inhibitor of TGF-β1 signaling (SB431542) and an antioxidant (*N*-acetylcysteine) had no effect (Figure 3B). LOXL2 enzymatic activity toward a model substrate was assessed monitoring H_2O_2 release. Corilagin blocked this activity with an IC_{50} of approximately 50 nM (Figure 3C). LOXL2-induced stabilization of Snail1 protein was also blocked by corilagin (Figure 3D). To test the possibility that the putative antioxidant activity of trihydrophenolics could either account for the observed inhibition of TGF-β1 signaling (38) or directly neutralize H_2O_2 in our LOXL2 enzyme assay, we defined the concentrations of corilagin that neutralized H_2O_2 activity in vitro (Supplemental Figure 4). We observed no inhibition of H_2O_2 interaction with a reporter substrate by corilagin at ≤10 μM, whereas vitamin C neutralized H_2O_2 at submicromolar concentrations, confirming that direct antioxidant scavenging activity could not account for our corilagin findings.

To assess inhibition of LOXL2 activity in vivo, we performed biochemical analyses of collagens obtained from primary 344SQ tumors of mice treated with EA or control chow (refs. 35, 39, and Figure 2A). Accumulation of cross-links including 2 reducible cross-links, HLNL and DHLNL, and a nonreducible, mature cross-link, deoxypyridinoline (DPD), was all significantly decreased in primary tumors of mice fed EA chow, consistent with the altered collagen organization in the primary tumors demonstrated by quantitative analysis of second-harmonic generation (Table 2 and Figure 2I), and confirming inhibition of cross-linking activity by trihydroxyphenolics in vivo. Long-term EA chow treatment (6 months) did not affect mouse total bone mineral density or collagen content in the aorta (Supplemental Figure 3, D–F), indicating that not all LOX family members were affected by the active compounds.

LOXL2 activity confers inhibition of TGF-β1 signaling by trihydroxyphenolics. To further interrogate the impact of LOXL2 inhibi-

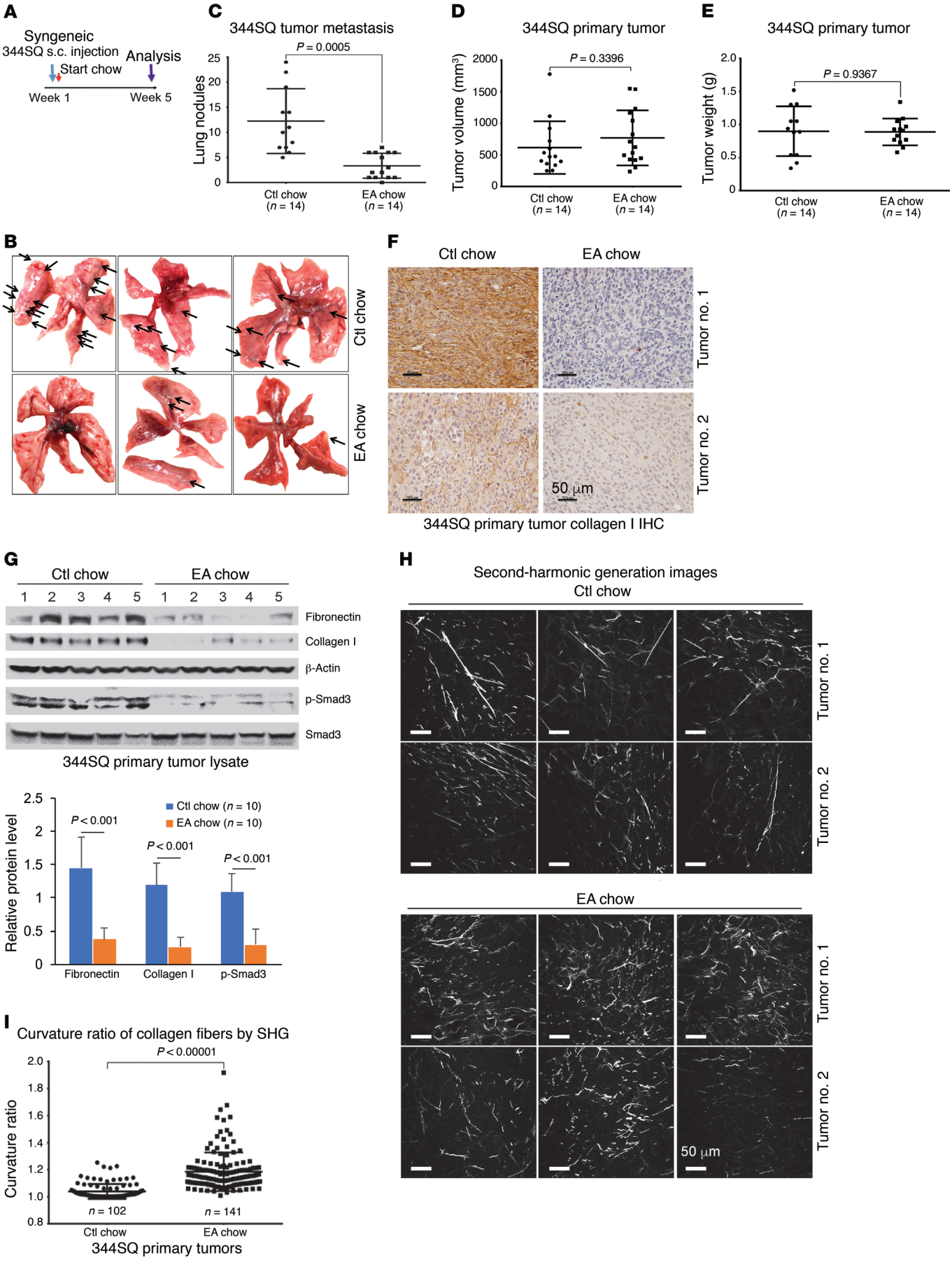
A
Syngeneic
344SQ s.c. injection
Start chow
Analysis
Week 1
Week 5
C
344SQ tumor metastasis
P = 0.0005
Lung nodules
Ctl chow (n = 14)
EA chow (n = 14)
D
344SQ primary tumor
P = 0.3396
Tumor volume (mm3)
Ctl chow (n = 14)
EA chow (n = 14)
E
344SQ primary tumor
P = 0.9367
Tumor weight (g)
Ctl chow (n = 14)
EA chow (n = 14)
B
Ctl chow
EA chow
F
Ctl chow
EA chow
Tumor no. 1
Tumor no. 2
50 μm
344SQ primary tumor collagen I IHC
G
Ctl chow
EA chow
1 2 3 4 5 1 2 3 4 5
Fibronectin
Collagen I
β-Actin
p-Smad3
Smad3
344SQ primary tumor lysate
Ctl chow (n = 10)
EA chow (n = 10)
P < 0.001
P < 0.001
P < 0.001
Relative protein level
Fibronectin
Collagen I
p-Smad3
H
Second-harmonic generation images
Ctl chow
EA chow
Tumor no. 1
Tumor no. 2
50 μm
I
Curvature ratio of collagen fibers by SHG
P < 0.00001
Curvature ratio
n = 102
n = 141
Ctl chow
EA chow
344SQ primary tumors

Figure 2. EA-rich diet attenuates 344SQ lung tumor metastasis and primary tumor collagen cross-linking. (**A**) Implantation and treatment in syngeneic lung cancer model. Metastatic 344SQ tumor cells were subcutaneously injected in syngeneic mice at 12 weeks old and treated with ctl or EA chow for 5 weeks. (**B**) Representative pictures of lung metastasis of 344SQ tumors treated with ctl or EA chow. (**C**) Quantification of lung metastasis of 344SQ tumors treated with ctl or EA chow (n = 14 mice per group). (**D**) Total volume of 344SQ tumors treated with ctl or EA chow (n = 14 mice per group). (**E**) Total tumor weight (grams) of ctl or EA chow–treated 344SQ primary tumors (n = 14 mice per group). (**F**) Collagen I immunohistochemistry (IHC) of 344SQ primary tumors treated with ctl or EA chow. Scale bars: 50 μm. (**G**) Ctl or EA chow–treated 344SQ primary tumors were lysed and immunoblotted for fibronectin, collagen I, β-actin, p-Smad3, and total Smad3. Quantification of bands normalized to β-actin was pooled from 10 mice per group. Data represent mean ± SD. Each protein was analyzed by 1-way ANOVA with a Tukey post hoc test. (**H**) Representative second-harmonic generation (SHG) images from 344SQ primary tumors treated with ctl or EA chow. Scale bars: 50 μm. (**I**) Quantification of curvature ratio for individual collagen fibers imaged by SHG microscopy of primary 344SQ tumor tissues treated with ctl (n = 102 collagen fibers per sample) or EA chow (n = 141 collagen fibers per sample). Data for **C**–**E** and **I** are expressed as mean ± SD. P value by unpaired 2-tailed t test.

tion on TGF-β1 responses, we suppressed LOXL2 levels with RNAi in A549 cells. Surprisingly, rather than inhibiting TGF-β1, silencing *LOXL2* completely abrogated the inhibitory effects of corilagin on TGF-β1–induced EMT in A549 cells (Figure 3E). Further, *LOXL2* but not *LOXL1* silencing in fibroblasts completely prevented the corilagin inhibitory effects on the TGF-β1–induced mesenchymal proteins N-cadherin, α-smooth muscle actin, and Snail1 (Figure 3F). These findings revealed that the corilagin mechanism of action was not simply LOXL2 inhibition, prompting us to revisit corilagin effects on TGF-β1 signaling.

Because trihydroxyphenolic compounds did not block TGF-β1–induced p-Smad generation in short-term assays (Figure 1C), we considered the possibility that impaired TGF-β1 signaling was due to defective p-Smad nuclear import, but immunostaining revealed no blockade of Smad2/3 nuclear translocation within 2 hours of compound treatment. However, longer preincubation of cells with corilagin (or other trihydroxyphenolics) for several hours completely suppressed Smad activation (Figure 4A and Supplemental Figure 5, A–C), implying that a degree of ongoing p-Smad generation is required for regulation of the TGF-β1 gene targets studied here (Figure 1H). Similarly, expression of LOXL2 in NMuMG cells that normally express very low levels of LOXL2 conferred corilagin responsiveness and blockage of p-Smad3 following 6-hour pretreatment (Figure 4B). Conversely, silencing *LOXL2* in A549 cells and primary lung fibroblasts completely blocked corilagin effects on p-Smad3 generation (Figure 4, C and D). Consistent with a critical role for LOXL2 in proximal TGF-β1 signaling, a survey of numerous cell lines revealed a direct correlation of *LOXL2* mRNA levels with the degree of inhibition of TGF-β1–induced Smad activation by corilagin (Supplemental Figure 6). To further test this principle in vivo, epithelial, fibroblast-rich mesenchymal, and immune cells were isolated by flow cytometry from pools of normal lungs and lungs of mice exposed 14 days earlier to bleomycin, then immediately stimulated with TGF-β1 and tested for their degree of p-Smad accumulation as a marker of TGF-β1 signaling (Figure 4E). There was a marked attenuation of p-Smad3 in the fibroblast-rich lung fraction of bleomycin-exposed mice also given oral epigallocatechin-3-gallate (EGCG; 100 mg/kg daily) but no discernible inhibition of p-Smad3 in either the epithelial or immune cell fractions. A second experimental design in which the isolated fractions from pools of normal lungs and lungs of mice exposed 14 days earlier to bleomycin fed with control or EA chow demonstrated the same pattern (Supplemental Figure 7), confirming the cell selectivity of trihydroxyphenolics on TGF-β1 signaling in vivo. Finally, we confirmed that inhibition of active LOXL2 by the copper chelator D-penicillamine (DPA) also abrogated corilagin effects on Smad activation and Snail1 induction (Figure 4F and Supplemental Figure 5, D–F). Together these data indicate that trihydroxyphenolic compounds selectively target proximal TGF-β1 signaling and Snail1 accumulation only in cells expressing LOXL2 and do so by a mechanism requiring the presence of active LOXL2.

To further investigate the specificity of trihydroxyphenolics for TGF-β1 signaling, we asked whether corilagin inhibited other kinases at 1–10 μM, well above the IC_{50} for its inhibitory effects on TGF-β1 signaling (Figure 1H). In a screen of 82 purified kinases conducted at the K_m for ATP binding for each kinase, only the tyrosine kinases EGFR and PDGFRβ were inhibited more than 50% at 1 μM (Supplemental Figure 8A). However, when we specifically tested the inhibitory effects of corilagin at 1 μM on either EGFR or PDGFRβ activities of intact cells, neither were inhibited by corilagin, implying that the cell-free kinase screen is more sensitive than the inhibition of these enzymes in intact cells (Supplemental Figure 8, B and C). These data confirm that corilagin is not a nonspecific kinase inhibitor, at least at concentrations less than or equal to 1 μM.

Trihydroxyphenolics induce auto-oxidation of LOXL2 lysine 731. Given the structural similarities between the trihydroxyphenolic motif and LTQ (Figure 3A), the results described above raised the possibility that the trihydroxyphenolic motif operates as an LTQ-like mimic, leading to its metabolism by LOXL2 and generating an inhibitor of TGF-β1 signaling. To begin testing this hypothesis we inspected the LOX catalytic domain for lysines specific to LOXL2 and not found in LOXL1 (Figure 5A), whose silencing had no impact on corilagin responsiveness (Figure 3F and Figure 4D).

Table 2. Collagen cross-links in 344SQ tumors treated with ctl or EA chow (moles per mole of collagen)

	Ctl chow, mean (±SD) (n = 3)	EA chow, mean (±SD) (n = 3)	Ctl vs. EA, P value
DHLNL	0.1 (0.00)	0.05 (0.01)	**0.005**
HLNL	0.39 (0.02)	0.25 (0.02)	**0.0015**
HHMD	0.23 (0.07)	0.14 (0.06)	0.26
PYD	0.19 (0.00)	0.26 (0.07)	0.33
DPD	0.039 (0.01)	0.022 (0.01)	**0.0221**

LOXL2 mediates the conversion of Lys to Lys^{ald}, which is ultimately processed to HHMD. LOXL2 also mediates the conversion of Hyl to Hys^{ald}. Hyl^{ald} can then be converted into DHLNL and subsequently PYD, Hyl^{ald} can be converted to HLNL and subsequently DPD. DHLNL, dehydro-dihydroxylysinonorleucine/its ketoamine; HLNL, dehydro-hydroxylysinonorleucine/its ketoamine; HHMD, dehydro-histidinohydroxymerodesmosine; Lys, lysine; Hyl, hydroxylysine; ald, aldehyde.

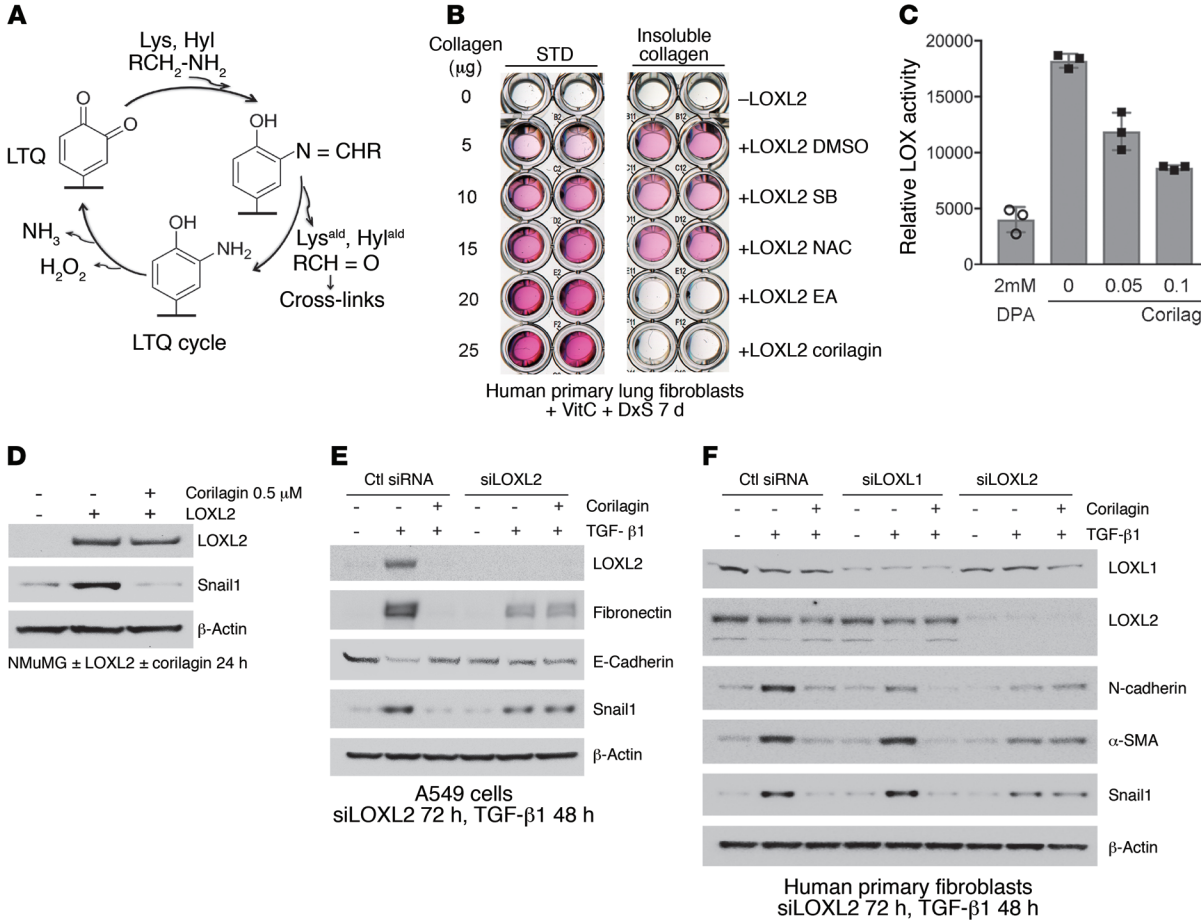

Figure 3. Identification of LOXL2 as the target of EA and corilagin; requirement for active LOXL2 for corilagin-induced inhibition of EMT and Snail expression. (**A**) LTQ cycle. LTQ converts lysine to allysine and yields an aminophenol intermediate. Subsequent hydrolysis release allysine and the original cofactor, producing hydrogen peroxide and ammonia as side products. (**B**) Primary human lung fibroblasts cultured in the presence of vitamin C and dextran sulfate were treated with recombinant human LOXL2 and different inhibitors for 7 days. The insoluble cross-linked collagen was extracted and measured by Sircol assay. SB, SB431542, TβRI inhibitor; NAC, *N*-acetylcysteine, antioxidant. STD, standard. (**C**) Recombinant human LOXL2 was incubated with 2 mM D-penicillamine (DPA) or different concentrations of corilagin (0–1 μM) for 1 hour, and LOX activity was measured. Data represent mean ± SD; $n = 3$. (**D**) NMuMG cells overexpressing human LOXL2 were incubated with or without 0.5 μM corilagin for 24 hours, lysed, and immunoblotted for LOXL2, Snail1, and β-actin. (**E**) A549 cells transfected with siRNA to LOXL2 were stimulated with TGF-β1 or left unstimulated for 48 hours in the presence or absence of 1 μM corilagin. The lysates were immunoblotted for LOXL2, fibronectin, E-cadherin, Snail1, and β-actin. (**F**) Primary human lung fibroblasts transfected with siRNAs to LOXL1 or LOXL2 were stimulated with TGF-β1 or left unstimulated for 72 hours in the presence or absence of 1 μM corilagin, and the lysates were immunoblotted for LOXL1, LOXL2, N-cadherin, α-smooth muscle actin (α-SMA), Snail1, and β-actin. **B** and **D**–**F** are representative of at least 3 experiments with similar results.

We then established and expressed Flag-tagged point mutants of each of 3 LOXL2/3–specific lysines, converting each to the corresponding LOXL1 residues: K614N, K731R, and K759R. Each of the point mutants had comparable enzyme activity to WT LOXL2 when expressed in NMuMG cells (Supplemental Figure 9A), and all except the K731 mutant were completely inhibited by corilagin (Figure 5B). Cells expressing K731R LOXL2 were completely resistant to inhibition of TGF-β1 signaling (Figure 5C) and Snail1 stabilization (Figure 5D) by corilagin, whereas the other mutants were indistinguishable from WT. Because lysine auto-oxidation by LOX family enzymes is critical to LTQ generation, we asked whether K731 was auto-oxidized to an aldehyde in the presence of corilagin. Incubation of a biotin hydrazide that covalently links to free aldehydes with immunoprecipitated WT and mutant LOXL2 confirmed that each enzyme except the K731R mutant developed an aldehyde when mixed with corilagin, implying that K731 but not other lysines is converted to an aldehyde during metabolism of corilagin by LOXL2 (Figure 5E).

A novel TβRI kinase inhibitor is generated inside LOXL2-expressing cells. We next screened compounds structurally similar to the intermediate aminophenol known to appear during the LTQ cycle (Figure 3A) for direct TGF-β1 inhibition. A catechol containing an amino group at position 3 (3Abd, 3-aminobenzene-1,2-diol) but not at either position 2 (2Abd) or 4 (4Abd) was found to be a potent inhibitor of TGF-β1–induced Smad3 activation and Snail1 expression without preincubation and regardless of LOXL2 expression (Figure 6, A–C, and Supplemental Figure 9B). We confirmed that 3Abd, but not control pyrogallol or 2Abd, directly blocked the kinase activity of recombinant TβRI catalytic domain with an IC_{50} of approximately 3 μM (Figure 6D and Supplemental Figure 9C), consistent with the inhibi-

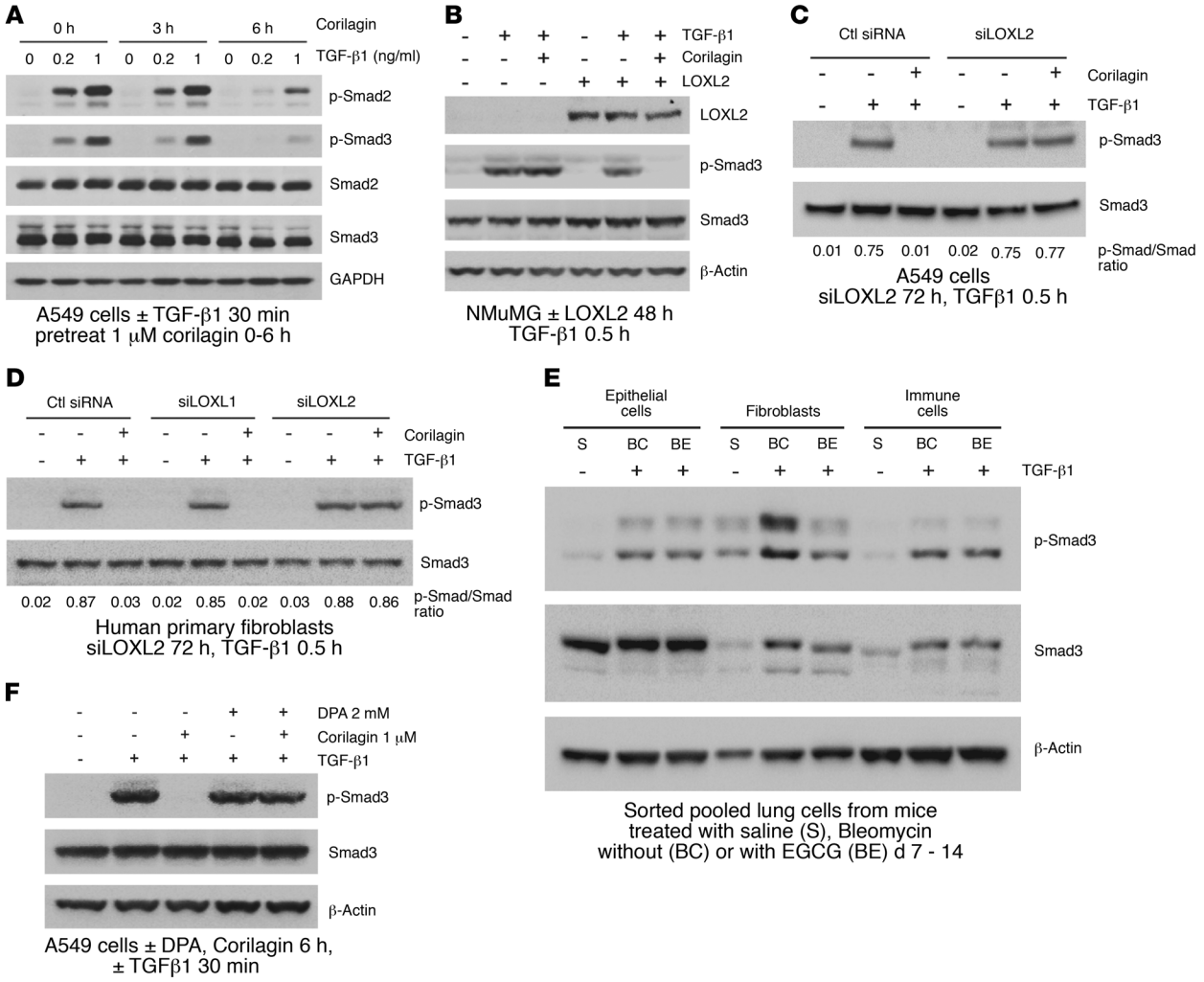

Figure 4. Corilagin inhibition of TGF-β1 signaling is dependent on LOXL2 activity. (**A**) A549 cells pretreated with 1 μM corilagin for 0, 3, or 6 hours were stimulated with different doses of TGF-β1 (0, 0.2, or 1 ng/ml) for 30 minutes, and the cell lysates were blotted for p-Smad2, p-Smad3, Smad2, Smad3, and β-actin. (**B**) NMuMG cells transfected with human LOXL2 or empty vector were pretreated with 1 μM corilagin or DMSO for 6 hours and then incubated without or with TGF-β1 for 30 minutes. The cell lysates were blotted for LOXL2, p-Smad3, Smad3, and β-actin. (**C** and **D**) A549 cells transfected with siRNA to LOXL2 (**C**) and primary human lung fibroblasts transfected with siRNAs to LOXL1 or LOXL2 (**D**) were pretreated with 1 μM corilagin or DMSO for 6 hours before incubation without or with TGF-β1 for 30 minutes. The cell lysates were blotted for p-Smad3 and Smad3. The ratio of p-Smad3/Smad3 for each lane is shown. (**E**) Mouse lung epithelial cells, fibroblasts, and immune cells sorted from mice treated for 14 days with saline (S), bleomycin with vehicle control (BC), or bleomycin with 7 days oral EGCG (100 mg/kg) (BE) were immediately treated with TGF-β1 for 30 minutes and cell lysates blotted for p-Smad3, total Smad3, and β-actin. $n = 5$ for each group. (**F**) A549 cells were pretreated with 1 μM corilagin with or without 2 mM DPA for 6 hours before TGF-β1 stimulation for 30 minutes. The cell lysates were blotted for p-Smad3, Smad3, and β-actin. The data from **A**–**D** and **F** are representative of at least 3 experiments with similar results.

tory profile of 3Abd in cells (Figure 6C). In cells overexpressing TβRI we also observed that 3Abd but not control 3Fc (3-Fluorocatechol) blocked the kinase activity of immunoprecipitated TGF-β receptors (Supplemental Figure 9D). Notably, 3Abd is structurally distinct from any of the known low–molecular weight inhibitors of TβRI (18).

To further define the mechanism of TGF-β1 inhibition by trihydroxyphenolic compounds, we asked whether secreted LOXL2 generated active 3Abd-like metabolites. Overnight coculture of corilagin-treated A549 cells with corilagin-nonresponsive NMuMG cells (Figure 4B) expressing a Smad3 reporter (12X CAGA) (40) revealed indistinguishable TGF-β1–induced reporter activation with or without 5-fold excess A549 cells in coculture, indicating that the generation of a diffusible inhibitor was unlikely (Figure 6E). In addition, lysates of corilagin-treated A549 cells, but not that of untreated cells, inhibited the kinase activity of immunoprecipitated TGF-β receptors (Figure 6F). These results point to an intracellular origin of a trihydroxyphenolic metabolite(s) inhibiting TβRI kinase (Figure 6G). While we demonstrated that the small fragment 3Abd that would result from a trihydroxyphenolic acting through an LTQ-like mechanism (and not pyrogallol) directly inhibits TβRI kinase (Figure 6D), future studies will be needed to isolate the exact inhibitory metabolite(s) present within trihydroxyphenol-treated LOXL2-expressing cells.

Discussion

These studies reveal, for the first time to our knowledge, a pathway of inhibition of the TGF-β1–induced collagen program selective to the cells that are most accountable for pathological collagen depo-

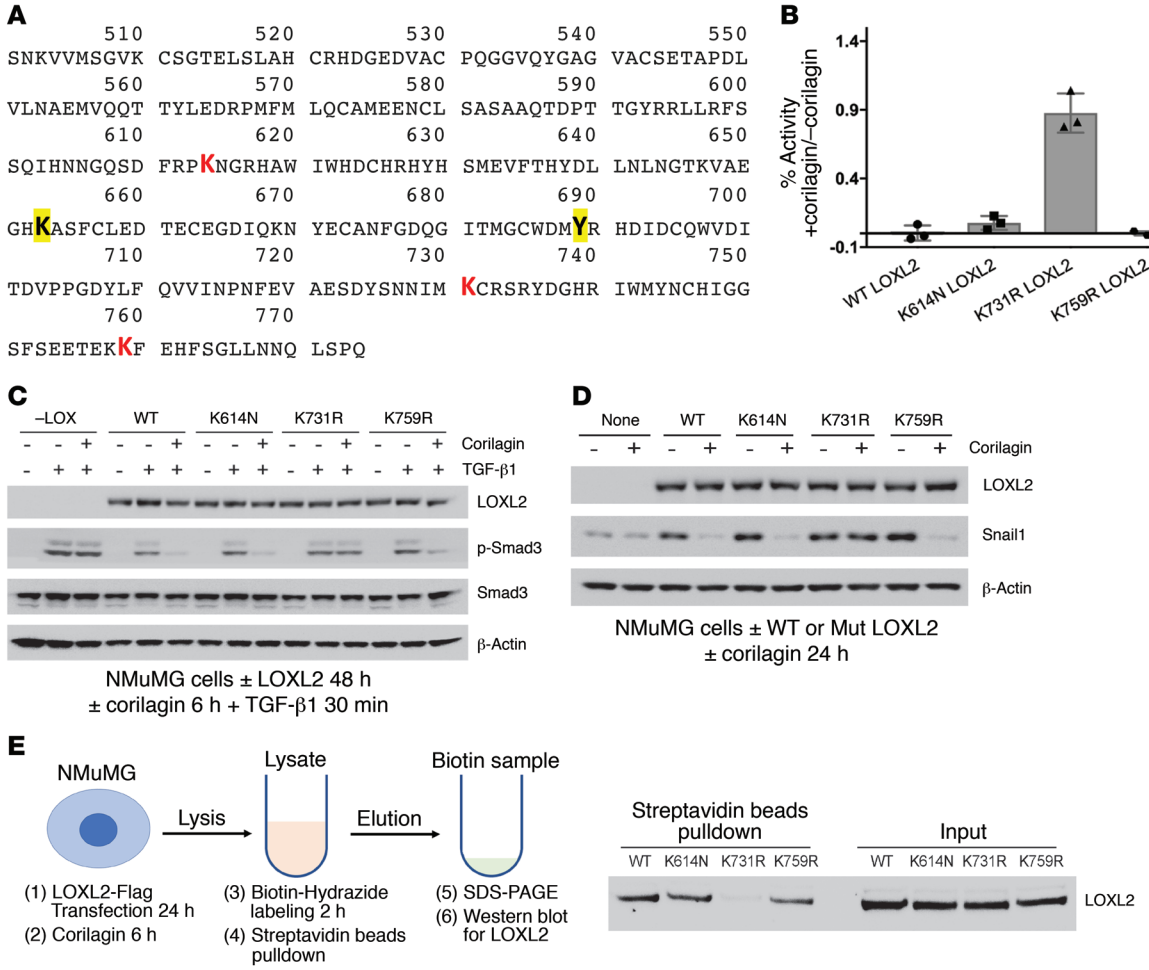

Figure 5. Trihydroxyphenolic motif mimics the LTQ, leading to auto-oxidation of LOXL2 K731 and inactivation of LOXL2. (**A**) Catalytic domain sequence of LOXL2. Catalytic domain: P548–S751. LTQ sites are highlighted and boldface (K653 and Y689). The 3 point mutation sites are in red (K614N, K731R, K759R). (**B**) NMuMG cells transfected with WT or mutant human LOXL2 were treated with 1 μM corilagin or DMSO for 6 hours. LOX activity of conditioned media from treated cells was measured. Data are presented as percent activity of no-corilagin control. Mean ± SD, $n = 3$. (**C**) NMuMG cells transfected with WT or mutant human LOXL2 were pretreated with 1 μM corilagin or DMSO for 6 hours and then incubated without or with TGF-β1 for 30 minutes. The cell lysates were immunoblotted for LOXL2, p-Smad3, Smad3, and β-actin. (**D**) NMuMG cells transfected with WT or mutant human LOXL2 were incubated with or without 1 μM corilagin for 24 hours, and lysates were immunoblotted for LOXL2, Snail1, and β-actin. (**E**) NMuMG cells transfected with WT or mutant human LOXL2 were incubated with 1 μM corilagin for 6 hours and labeled with 2.5 mM biotin hydrazide for 2 hours. The biotin hydrazide–linked carbonylated LOXL2 was pulled down with streptavidin–magnetic beads, and the precipitates and input protein were immunoblotted for LOXL2. **C**–**E** are representative of at least 3 experiments with similar results.

sition, tissue fibroblasts and fibroblast-like tumor cells. The surprising finding that such selectivity depends on active LOXL2/3 and appears to operate in a cell-autonomous manner largely abrogates inhibition by trihydroxyphenolic-containing compounds of TGF-β1 signaling in epithelial or immune cells that don't express LOXL2/3. This selectivity likely avoids the toxicities of long term general TGF-β1 inhibition in chronic disease processes such as fibrosis and cancer progression. Indeed, we have observed no adverse events in mice on the trihydroxyphenolic-rich diet (EA chow) for at least 6 months, including the absence of skin inflammation and discernible lesions in cardiac valves. Likewise, none of the compounds tested here had any negative effects on cell viability in vitro at concentrations up to 10 μM of trihydroxyphenolics or 50 μM of 3Abd (Supplemental Figure 10). The selective inhibition of intracellular and extracellular LOXL2/3 by trihydroxyphenolics also distinguishes this mechanism of LOX family inhibition from that of previously described extracellular LOXL2 inhibitors as well as global LOX inhibitors, accounting for the lack of negative impact of long-term exposure to EA-rich compounds on bone or vascular collagen content (Supplemental Figure 3, D–F, and refs. 34, 41). Maintenance of musculoskeletal and vessel wall collagen and elastin integrity depends on LOX and LOXL1, not LOXL2 (42–45). Although selective, the combined inhibition of LOXL2 and TGF-β1 signaling in fibroblast-like cells results in potent in vivo antifibrotic activity that has untapped but promising potential as a therapeutic approach for chronic diseases such as pulmonary fibrosis dominated by progressive collagen accumulation.

The combined inhibition of LOXL2 and TGF-β1 signaling in fibroblast-like cells could be expected to impact biomarkers of collagen turnover in vivo. Indeed, we observed an increase in urinary levels of pyridinoline (PYD) and DPD, nonreducible end products of cross-linked collagen metabolism, in mice 10–21 days after

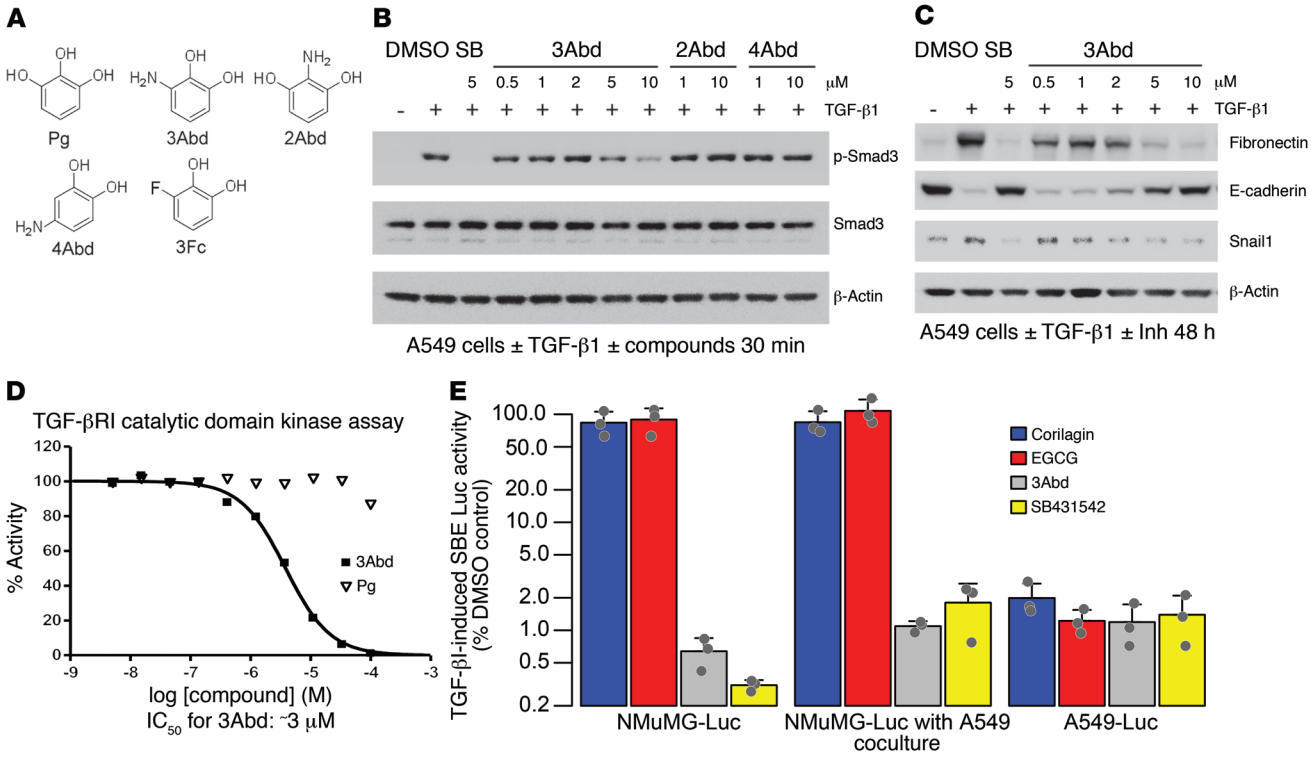

Figure 6. Generation of a novel nondiffusible TβRI kinase inhibitor. (**A**) Structure of pyrogallol (Pg), 3Abd, and derivatives. (**B**) A549 cells were stimulated with TGF-β1 for 30 minutes and lysates immunoblotted for p-Smad3, Smad3, and β-actin. Treatment without preincubation: 3Abd (0.5–10 μM); 2Abd or 4Abd (1, 10 μM). (**C**) A549 cells were stimulated with TGF-β1 for 48 hours and lysates immunoblotted for LOXL2, fibronectin, E-cadherin, Snail1, and β-actin. 3Abd was added at concentraions ranging from 0.5 to 10 μM. (**D**) Purified ALK5/TβRI catalytic domain kinase assay was performed with 10 doses of 3Abd or Pg starting from 100 μM. Kinase activity was indicated by ^{33}P-ATP signals, and IC_{50} of 3Abd was calculated as approximately 3 μM. **B**–**D** are representative of 3 experiments with similar results. (**E**) SMAD-binding element (SBE) reporter–transfected NMuMG and A549 cells were seeded into a 96-well plate. Cocultured wells were seeded with 5,000 transfected NMuMG cells and 25,000 nontransfected A549 cells. Cells were pretreated with or without 1 μM corilagin, 1 μM EGCG, 10 μM 3Abd, or 5 μM SB431542 for 6 hours and stimulated with TGF-β1 overnight before lysis for luciferase assay. Data are presented as percent TGF-β1–induced SBE luciferase activity of DMSO control in log scale. Mean ± SD, $n = 3$. (**F**) Flag-tagged TβRI and TβRII were immunoprecipitated from A549 cells and in vitro kinase assay performed on beads exposed to lysate pretreated with corilagin or DMSO. The final reaction was eluted and analyzed by immunoblotting for phosphotyrosine and TβRI. The phosphotyrosine bands were quantified using ImageJ and normalized to DMSO control. Data represent mean ± SD. *P* value by unpaired 2-tailed *t* test of 6 separate experiments. (**G**) Schematic overview of mechanism. A trihydroxyphenolic-containing compound engages active LOXL2, initiating auto-oxidation of K731 and creating a key allysine inactivating the enzyme. In the process, a 3Abd-like metabolite is generated that then blocks TβRI kinase. The combined effects block pathological collagen accumulation.

bleomycin injection, and this increase was suppressed by treatment of the mice with corilagin (Supplemental Figure 11A). Consistent with these findings, we observed increased mean urinary PYD/DPD levels in 2 cohorts of patients with idiopathic pulmonary fibrosis (Supplemental Figure 11B), suggesting that a signal from fibrotic lungs is present in most of these patients and may enable tracking of collagen turnover and drug responses in vivo.

The biological pathway identified here uses trihydroxy-containing polyphenols at concentrations achievable by dietary ingestion. Indeed, foods rich in this class of compounds, such as EGCG (the major polyphenol in green tea), have been consumed as therapeutics for decades (46). Yet these compounds are not generally thought of as workable drugs because of their potential for pro- and antioxidant reactions that could negatively impact pathways, such as drug metabolism, sensitive to such reactions (47). The designation of these polyphenols as antioxidants and as reactive compounds, however, largely stems from prior studies that have used micromolar levels of polyphenols to achieve in vitro "antioxidant" or signaling inhibition in multiple cell systems (48), even though blood levels above approximately 150 nM have not been documented for dietary polyphenols consumed by humans (49–53). As well, we observed no neutralization of H_2O_2 oxidant activity by corilagin at concentrations below 10 μM (Supplemental Figure 4). We believe the LOXL2-dependent interaction with trihydroxyphenolics is a singular example of a relevant protective pathway activated by nanomolar levels of the relevant ellagitannin and catechin subclasses, possibly contributing to the observed beneficial effects of green tea and other trihydroxyphenolic-rich diets in numerous population studies (54–56).

Methods

Reagents. Ellagic acid (EA; E2250), epigallocatechin gallate (EGCG; E4143), epicatechin gallate (E3893), epigallocatechin (EGC; E3768), gallocatechin (E3768), epicatechin (EC; E1753), catechin (C1251), luteolin (L9283), chloramine T (857319), *p*-dimethylaminobenzaldehyde (156477), bleomycin (B5507), D-penicillamine (DPA; P4875), pyrogallol (254002), *N*-acetylcysteine (A7250), protease inhibitor cocktail (P8340), phosphatase inhibitor cocktail (P5726), fibronectin polyclonal antibody (pAb) (F3648), α-smooth muscle actin mAb (A5228), Flag M2 mAb (F3165), and β-actin mAb (A5441) were purchased from Sigma-Aldrich. Corilagin (23094-69-1) was purchased from BOC Sciences. TGF-β type I receptor inhibitor SB431542 (S4317), phospho-Smad2 (Ser465/467) pAb (566415), EGFR pAb (06-847), and phosphotyrosine mAb 4G10 (05-321) were from EMD Millipore. Snail1 mAb (3895), Smad2 mAb (5339), phospho-Smad1/5 (Ser463/465) pAb (9516), Smad1 pAb (9743), phospho-EGFR pAb (2231), phospho-PDGFRβ pAb (3161), and PDGFRβ Rb mAb (3169) were from Cell Signaling Technology. Collagen I pAb (ab292), vimentin mAb (ab45939), LOXL2 pAb (ab96233) for Western blot, and phospho-Smad3 (Ser423/425) pAb (ab52903) were from Abcam. SiRNAs for human LOXL1 (sc-45220) and LOXL2 (sc-45222) and secondary HRP-conjugated antibodies (mouse, sc-2005; rabbit, sc-2004) were from Santa Cruz Biotechnology. Streptavidin–magnetic beads (11205D), TurboFect transfection reagent (R0531), and EZ-Link Hydrazide-LC-Biotin (PI21340) were from Thermo Fisher Scientific. Protein G–agarose (11719416001) was from Roche. E-cadherin (610182) and N-cadherin (610921) antibodies were from BD Biosciences. TGF-β1 (100-21) was from PeproTech. 3-Aminobenzene-1,2-diol (3Abd; W4593) was from Aurum Pharmatech Inc. 2-Aminobenzene-1,3-diol (2Abd; 23488), 4-aminobenzene-1,2-diol (4Abd; 31975), and 3-fluorocatechol (CL8492) were from AstaTech Inc. Human recombinant LOXL2 (2639-AO-010) was purchased from R&D Systems.

Cell culture. Human or mouse cell lines were purchased from ATCC and grown in DMEM or RPMI 1640 medium supplemented with L-glutamine and 10% FBS (Hyclone). Human and mouse lung fibroblasts were isolated from crude whole-lung single-cell suspension cultures on Petri dish in DMEM supplemented with L-glutamine and 10% FBS for 2 weeks. Mouse type II alveolar epithelial cell isolation and culture were performed as previously described (57). All the cell lines in the laboratory are periodically tested for mycoplasma contamination. Only the mycoplasma-free cells are used for experiments.

High-throughput screen and high-content imaging analysis. A549 cell–based screening for inhibitors of TGF-β1–induced EMT from small-molecule libraries was performed in 384-well plate format, and the images were captured and analyzed using GE IN Cell 2000 as described previously (26).

Immunofluorescence. Cultured cells and 5- to 7-μm cryosections were fixed in 4% paraformaldehyde and stained with various antibodies and IgG isotype controls. Where indicated in the figure legends, mosaic images were generated from multiple ×20 images captured on a Zeiss Axio upright fluorescent microscope and tiled using 10% image overlap by Axiovision 4.7 software (Zeiss).

Masson's trichrome stain. For histological assessment of lung collagen, frozen sections of the left lung were stained using Masson's trichrome stain kit (22-110-648, Thermo Fisher Scientific). The whole section was imaged with a Zeiss Axio upright microscope and tiled using 10% image overlap into a single panoramic by Axiovision 4.7 software (Zeiss).

Immunoblot. Pulverized tissue and cells were lysed in RIPA buffer (150 mM NaCl, 50 mM Tris, pH 8.0, 1% Triton X-100, 0.5% sodium deoxycholate, 0.1% SDS, supplemented with protease and phosphatase inhibitors) and analyzed by immunoblotting. Densitometry was quantified using NIH ImageJ software. See complete unedited blots in the supplemental material.

Bleomycin fibrosis model. Eight-week-old C57BL/6 mice were intratracheally instilled with saline or 1.9 units/kg of bleomycin (Sigma-Aldrich). Mice were implanted with Alzet osmotic pumps (1007D, DURECT Corp.) loaded with EA salt (24 mg/kg/d, days 10–17), fed with red raspberry diet (EA chow, days 0–21), or gavaged with corilagin (100 mg/kg, days 10–21). Controls were treated with control pump, control diet, or vehicle in the same formulation. Red raspberry diet (TD.130761) and red control diet (TD.150279) was custom-made by Envigo. The lungs were lavaged, and then embedded in OCT compound for imaging or snap-frozen in liquid nitrogen for protein extraction or hydroxyproline assay.

Syngeneic in vivo tumorigenesis and metastasis assays. KrasG12D/p53R172H metastatic lung cancer cells (344SQ) were subcutaneously injected in the right flanks of male, syngeneic 129/Sv mice at 3 months of age and allowed to form tumors for 5–6 weeks (29). The mice were fed with red raspberry diet or control diet. After euthanasia, tumors were measured and lung metastatic nodules were quantified. Primary tumor tissues were snap-frozen and analyzed by Western blot. Some primary tumors were formalin fixed, paraffin embedded, and sectioned for immunohistochemistry or second-harmonic generation imaging. The investigators were completely blinded to drug treatment and outcome assessment.

Immunohistochemistry and second-harmonic generation microscopy. Paraffin-embedded tissue sections were rehydrated, blocked with goat serum, and probed for collagen I. Tissues were subsequently washed and probed with HRP-conjugated secondary antibodies, and signal was attained by developing with a DAB reagent. Collagen cross-linking alteration was evaluated by second-harmonic generation microscopy. Tissues stained by H&E were visualized using a Zeiss LSM 7 MP Multiphoton Microscope at an excitation wavelength of 800 nm, and collagen fiber signals were detected at 380–430 nm using bandpass filters. Collagen linearity was calculated as a ratio of the total length versus the end-to-end length of the individual collagen fiber.

Collagen content. Lung or aorta collagen content was evaluated using hydroxyproline assay (58). Briefly, whole left lung tissue or aorta was hydrolyzed in 1 ml 12N HCl at 110°C for 24 hours, the hydroxyproline was detected by incubation with chloramine T and *p*-dimethylaminobenzaldehyde, and the absorbance was measured at 550 nm. Each sample was run in triplicate. Collagen content in lung or aorta tissues was expressed as micrograms of collagen per lung or aorta and was converted from micrograms of hydroxyproline.

Bronchoalveolar lavage. After the trachea was exposed, a 20-gauge catheter was inserted into the trachea through a small incision. One milliliter cold PBS was instilled into the mouse lungs followed by gentle aspiration, and this was repeated 2 more times. All the bronchoalveolar lavage fluid (BALF) was centrifuged, and the cell pellet was resuspended in erythrocyte (rbc) lysis buffer (Sigma-Aldrich) followed by recentrifugation. Cell number was counted using a hemocytometer. Cell types of BALF were determined by morphology following Diff-Quik stain of cytospin slides. About 500 cells were counted for each sample in order to determine the cell types. Macrophages account for more than 80% of the cells in BALF and were collected by centrifugation. After centrifugation, the supernatant was collected to measure total protein content using the BCA assay (23225, Pierce), while the cell pellet was lysed for immunoblotting or RNA isolation.

Plasma level of corilagin. Plasma level of corilagin in C57BL/6 mice 2 hours following the last oral administration at day 21 was analyzed by Quintara Discovery. Blood samples (~500 μl/sample) were collected via cardiac puncture. Samples were placed in tubes containing heparin sodium and stored on ice until centrifuged for plasma.

Preparation of insoluble cross-linked collagen. Fibroblasts were cultured on a 10-cm dish until confluent. The medium was then changed to DMEM containing 5% FBS, 100 μM L-ascorbic acid with 500 kDa dextran sulfate at 100 μg/ml, and 50 ng/ml recombinant human LOXL2 for 7 days (36, 37). The cell layer was extracted with 0.5 M acetic acid and 0.1 mg/ml pepsin overnight at 4°C. The leftover insoluble fraction was further extracted and the insoluble cross-linked collagen measured using Sircol Insoluble Collagen Assay kit (S1000, Biocolor) according to the manufacturer's instruction.

LOX activity assay. LOX activity of recombinant human LOXL2 or conditioned medium collected from cells expressing LOXL2 was measured using a Fluorometric Lysyl Oxidase Activity Assay Kit (ab112139, Abcam) following a protocol provided by the manufacturer. Briefly, 50 μl of sample was mixed with an equal volume of assay reaction mixture containing LOX substrate, HRP, and HRP substrate in the presence and absence of testing inhibitors and D-penicillamine (DPA), a LOX inhibitor. The mixture was incubated for 30 minutes at 37°C in darkness. The fluorescence increase was then measured with a fluorescence plate reader (BMG LabTech FLUOstar) at excitation (Ex)/emission (Em) = 540/590 nm. Sample buffer or medium alone without LOXL2 was used for determination of the background fluorescence.

Collagen cross-link analysis. Snap-frozen primary 344SQ tumors were pulverized in liquid nitrogen using a Spex Freezer Mill (Spex), washed with cold PBS and cold distilled water, lyophilized, and weighed. Aliquots were reduced with standardized NaB^3H_4 and hydrolyzed with 6N HCl. The hydrolysates were then subjected to amino acid and cross-linking analyses using liquid chromatography–tandem mass spectrometry (LC–MS/MS) as described previously (59). The terms DHLNL, HLNL, and HHMD represent both the unreduced and reduced forms. The mature trivalent cross-links, PYD and DPD, were simultaneously analyzed by their fluorescence. All cross-links were quantified as the moles per mole collagen based on the value of 300 residues of hydroxyproline per collagen molecule.

Urinary PYD/DPD measurements. Pooled urine from each of 3–5 mice for each time point after bleomycin in a cohort of mice treated with vehicle or corilagin (100 mg/kg) beginning on day 10 after bleomycin was collected. Urine specimens were also collected from 2 cohorts of idiopathic pulmonary fibrosis patients and controls at 2 sites: The University of Texas Health Science Center at San Antonio and UCSF. All consenting patients with physician-established diagnosis of idiopathic pulmonary fibrosis followed in the respective interstitial lung disease (ILD) programs were included in sample collection. PYD/DPD levels from all the samples were measured using MicroVue EIA Assay Kit (catalog 8010) and MicroVue Creatinine EIA Kit (catalog 8009, Quidel Corp.) along with PYD/DPD standards, and the results were normalized relative to urinary creatinine. The statistical significance of human urine samples was analyzed using Mann-Whitney *U* test.

Bone mineral density measurement. Bone mineral density of mice treated with red raspberry diet or control diet up to 6 months was measured using dual-energy X-ray absorptiometry (DEXA) scan. DEXA scans were performed using the Lunar PIXImus Densitometer (GE Medical Systems) at the UCSF animal facility. The PIXImus Densitometer was calibrated before each testing using a quality control phantom following the manufacturer's instructions.

Elastic Van Gieson stain. Aortas isolated from mice treated with red raspberry diet or control diet up to 6 months were embedded in paraffin (n = 3 per group). Sections (5 μm) were cut every 30 μm along the aortas (starting from the proximal end). Selected sections were stained with Miller's Elastica Van Gieson stain.

Site-directed mutagenesis of LOXL2. Site-directed mutagenesis was performed to generate K614N, K731R, and K759R point mutations using Phusion Site-Directed Mutagenesis Kit (F541, Thermo Fisher Scientific) according to the manufacturer's instructions. A pcDNA3-hLOXL2-Flag plasmid containing the cDNA fragment of WT human LOXL2 fused with a Flag tag at the C-terminus (gift from Amparo Cano, Instituto de Investigaciones Biomédicas, Universidad Autónoma de Madrid/Consejo Superior de Investigaciones Científicas, Madrid, Spain) (30) was used as the template DNA (30). Mutations were confirmed by DNA sequencing. The primers and their complementary strands used were: K614N forward 5′-GACTTCCGGCCTAATAATGGCCGC-3′, K614N reverse 5′-GGACTGGCCATTGTTGTGGATCTG-3′; K731R forward 5′-ACAACATCATACGATGCAGGAGCC-3′, K731R reverse 5′-TGGAGTAATCGGATTCTGCAACCT-3′; K759R forward 5′-ACGGAAAAACGTTTTGAGCACTTCA-3′, and K759R reverse 5′-CTCTTCGCTGAAGGAACCACCTAT-3′.

Biotin hydrazide derivatization of carbonylated LOXL2. NMuMG cells were transiently transfected with WT or mutant human LOXL2-Flag in a 10-cm dish, and 24 hours later the cells were treated with 1 μM corilagin for 6 hours at 37°C before lysis in 50 mM HEPES, 100 mM NaCl, 2 mM EDTA, 0.5% Triton-100 plus protease inhibitor cocktail, 10 mM NaF, 1 mM Na_3VO_4. The lysates were incubated with 2.5 mM EZ-Link Hydrazide-LC-Biotin in the dark for 2 hours at room temperature. Biotin hydrazide–bound proteins were captured using streptavidin–magnetic beads (Pierce) on a rotary mixer at 4°C overnight. The beads were washed 3 times with lysis buffer and eluted with sample buffer for 10 minutes at 70°C. Biotin hydrazide–linked carbonylated LOXL2 and total input LOXL2 were detected by LOXL2 polyclonal antibody or Flag monoclonal antibody (M2) blot.

In vitro TGF-β receptor kinase assay. A549 cells were transiently cotransfected with Flag-tagged human TGF-β receptor I and II. After 24 hours the cells were lysed in 1% NP-40 lysis buffer (1% NP-40, 20 mM Tris, pH 7.6, 200 mM NaCl plus protease inhibitor cocktail, 10 mM NaF, 1 mM Na_3VO_4), and the type I and II receptors were immunoprecipitated using anti-Flag antibody and Protein G–Agarose (Roche). The beads were washed 3 times with kinase buffer (0.01% Triton X-100, 25 mM HEPES, pH 7.4, 2 mM $MnCl_2$, 10 mM $MgCl_2$, 20 μM DTT, 0.1 mM NaF, 0.1 mM Na_3VO_4). The kinase reactions were initiated by addition of 0.1 mM ATP in the presence or absence of inhibitors or lysate from A549 cells pretreated with corilagin (1:10 dilution into kinase reaction). The kinase reactions were terminated by addition of an equal volume of 2× sample buffer. The TGF-β receptor kinase activity was analyzed by SDS-PAGE and immunoblotting with anti-phosphotyrosine monoclonal antibody 4G10 and anti-Flag antibody.

ALK5/TβRI catalytic domain kinase assay. ALK5/TβRI kinase assays using purified catalytic domain were performed by Reaction Biology Corp. The reaction buffer contained 20 mM HEPES, pH 7.5, 10 mM $MgCl_2$, 1 mM EGTA, 0.02% Brij35, 0.02 mg/ml BSA, 0.1 mM Na_3VO_4, 2 mM DTT, and 200 μM *N*-acetylcysteine. In brief, ten 3-fold series dilutions of 3Abd and control pyrogallol or 2Abd starting at 100 μM were delivered into kinase reaction mixture with kinase, cofactors, and substrate. After 20 minutes of incubation at room temperature, ^{33}P-ATP was delivered into the mixture to initiate the reaction. Kinase activity was detected 2 hours later by P81 filter-binding method.

Coculture SMAD-binding element reporter. NMuMG and A549 cells were transiently transfected with pGL$(CAGA)_{12}$Luc using Turbofect reagent as specified by the manufacturer (Thermo Fisher Scientific). The transfected cells were seeded into a 96-well plate in triplicates 24 hours after transfection. Cocultured wells were seeded with transfected NMuMG cells and nontransfected A549 cells (1:5 ratio). The cells were pretreated with or without 1 μM corilagin, 1 μM EGCG, 10 μM 3Abd, or 5 μM SB431542 for 6 hours before stimulation with TGF-β1 overnight. The cells were lysed and luciferase activity was measured using the luciferase assay kit (E4030) from Promega.

Quantitative reverse transcription PCR analysis. Total RNA (1 μg of each sample isolated using RNeasy Kit, 74004, Qiagen) was reverse transcribed using SuperScript III (18080-051, Invitrogen) and assayed for gene expression using Platinum Quantitative PCR SuperMix-UDG (11730-025, Invitrogen). β-Actin, *Gapdh*, and *S9* were used as internal controls, and all the data were normalized by β-actin. The primer and probe sequences are listed in Supplemental Table 1.

Mouse lung cell sorting and analysis. Mouse lung single-cell preparations were performed as previously described (57). Single cells were incubated for 1 hour at 4°C with the following primary antibodies: rat anti–mouse CD45–APC-Cy7 (1:100; BD, 557659), rat anti–mouse PeCAM–PE (1:100; BD, 553373), rat anti–mouse EpCAM–Alexa Fluor 488 (1:250; BioLegend, 118210), and viability dye Sytox blue (1:1,000; Thermo Fisher Scientific, S34857). Cell sorting was performed on BD FACS Aria cytometers. $EpCAM^+$ and $CD45^+$ cells were collected, respectively. EpCAM/CD45/CD31–triple-negative cells were collected as mesenchymal cells. Each of the 3 cell types sorted from saline control, bleomycin control, and bleomycin EGCG groups ($n = 5$) were lysed and blotted for p-Smad3 and total Smad3.

Protein and lipid kinase screen. Protein kinase assays were conducted using the KinaseProfiler service of Eurofins Pharma Discovery Services UK Ltd. The kinase of interest was incubated with the test compound in assay buffer containing substrate, 10 mM magnesium acetate, and [γ-^{33}P-ATP]. The reaction was initiated by the addition of the Mg/ATP mix. After incubation at room temperature, the reaction was stopped by the addition of a 3% phosphoric acid solution. An aliquot of the reaction was then spotted onto a filtermat and washed in phosphoric acid followed by a rinse in methanol prior to drying and scintillation counting. Results were expressed in relation to controls containing DMSO only in place of test compound. The ATP concentration in each assay was within 15 μM of the determined apparent K_m for ATP.

Lipid kinase assays were conducted using the KinaseProfiler service of Eurofins Pharma Discovery Services UK Ltd. The kinase of interest was incubated in assay buffer containing substrate and Mg/ATP. The reaction was initiated by the addition of the Mg/ATP solution. After incubation for 30 minutes at room temperature, the reaction was stopped by the addition of stop solution containing EDTA and a biotinylated form of the reaction product. Finally, detection buffer was added, containing europium-labeled anti-GST monoclonal antibody, a GST-tagged lipid binding domain, and streptavidin-conjugated allophycocyanin. The plate was then read in time-resolved fluorescence mode, and the homogeneous time-resolved fluorescence (HTRF) signal was determined according to the formula HTRF $= 10{,}000 \times (Em_{665nm}/Em_{620nm})$.

H_2O_2 scavenging assay. The oxidant scavenging activity of corilagin and vitamin C was measured using Amplex Red Hydrogen Peroxide/Peroxidase assay kit (Thermo Fisher Scientific, A22188) following the manufacturer's instructions. H_2O_2 (0.5 μM) samples were incubated with different concentrations of corilagin (0–100 μM) and vitamin C (0–10 μM) for 2 hours at room temperature before Amplex Red/HRP reaction and the plate read at Ex/Em 540/590 nm with a fluorescence plate reader (BMG LabTech FLUOstar). Compound vehicle was used for determination of the background fluorescence. Experiments were performed in triplicate, and data are presented as means ± SD.

Cell viability assay. AlamarBlue cell viability reagent (Thermo Fisher Scientific, DAL1025) was used to assess cell viability. A549 or human primary lung fibroblasts (20,000 cells) in complete RPMI or DMEM medium were seeded into a 96-well tissue culture plate overnight; then the cells were exposed to different compounds for 72 hours. AlamarBlue reagent (1:10) was added to the cells, followed by 2 hours of incubation at 37°C, and absorbance at 570 nm was measured. Experiments were performed in triplicate using different batches of cells, and data are presented as means ± SD.

Statistics. Descriptive statistics are reported as means ± SD. For evaluation of differences between compound treated and control groups, the unpaired 2-tailed Student's *t* test or Mann-Whitney *U*

test was used assuming equal variance. Comparisons among multiple treatments were performed via 1-way ANOVA for repeated measures. Differences between groups were assessed with Tukey's multiple comparison tests. A P value less than 0.05 was accepted as significant. Two-tailed Spearman's rho calculation was used to assess the correlations. The survival of bleomycin-treated mice was analyzed by χ^2 test.

Study approval. All mice were maintained under specific pathogen–free conditions at UCSF according to IACUC protocol AN109566 and at MD Anderson Cancer Center according to IACUC protocol 00001271. For human subjects, written informed consent was obtained from each patient in accordance with the ethics guidelines for research in the US (protocols 10-02400 and 12-09662, approved by the IRB committee of UCSF, and protocol HSC20110086H, approved by the IRB committee of The University of Texas Health Science Center at San Antonio).

Author contributions

YW designed and performed experiments, analyzed the data, and wrote the manuscript. TJK performed most of the in vitro and in vivo experiments with the lung fibrosis model. DHP performed in vivo experiments with the tumor metastasis model and analyzed data. DD performed in vitro TGF-β1 signaling experiments and conducted kinase assays. DLG provided expertise in tumor metastasis. MY analyzed collagen cross-links in tumors. JRJ assisted with in vivo experiments. CJL, CC, and JP measured mouse and human urinary PYD and analyzed data. RD provided expertise in the TGF-β1 pathway and critical revision of the manuscript. BJB provided expertise in chemical structure-activity relationship and support on experimental design. HAC designed and oversaw the study and wrote the manuscript.

Acknowledgments

This work was supported by NIH PO1 HL108794 (to HAC), Cancer Prevention Research Institute of Texas (CPRIT) grant RP120713 P2 (to DLG), and CPRIT Graduate Scholar Training Grant RP140106 (to DHP). The authors thank Steve Chen from UCSF Small Molecule Discovery Center for assistance with high-throughput screening, Reaction Biology Corp. for performing the TβRI catalytic domain kinase assay, Eurofins Pharma Discovery Services UK Ltd. for performing protein and lipid kinase assays, David Morgan at Pliant Therapeutics for assistance with the kinase screen, and Julie Ren from Quintara Discovery for analyzing LC-MS/MS data. We thank Amparo Cano from Instituto de Investigaciones Biomédicas, Madrid, Spain, for LOXL2 construct. We also thank Ying Xi, Kevin Tan, and Alexis Brumwell for technical assistance, Joyce Lee from the University of Colorado (Denver, Colorado, USA) for providing human urine samples for analysis, and Anoop M. Nambiar for recruiting human subjects.

Address correspondence to: Ying Wei or Harold A. Chapman, Pulmonary and Critical Care Division, University of California at San Francisco, 513 Parnassus Avenue, San Francisco, California 94143-0130, USA. Phone: 415.514.1210; E-mail: ying.wei@ucsf.edu (Y. Wei); hal.chapman@ucsf.edu (H.A. Chapman).

1. Thannickal VJ, Zhou Y, Gaggar A, Duncan SR. Fibrosis: ultimate and proximate causes. *J Clin Invest*. 2014;124(11):4673–4677.
2. Friedman SL, Sheppard D, Duffield JS, Violette S. Therapy for fibrotic diseases: nearing the starting line. *Sci Transl Med*. 2013;5(167):167sr1.
3. Bartram U, Speer CP. The role of transforming growth factor beta in lung development and disease. *Chest*. 2004;125(2):754–765.
4. Han CY, et al. Hepcidin inhibits Smad3 phosphorylation in hepatic stellate cells by impeding ferroportin-mediated regulation of Akt. *Nat Commun*. 2016;7:13817.
5. Hu C, et al. Regulation of TGFbeta1-mediated collagen formation by LOX-1: studies based on forced overexpression of TGFβ1 in wild-type and lox-1 knock-out mouse cardiac fibroblasts. *J Biol Chem*. 2008;283(16):10226–10231.
6. Sheppard D. Transforming growth factor β: a central modulator of pulmonary and airway inflammation and fibrosis. *Proc Am Thorac Soc*. 2006;3(5):413–417.
7. Principe DR, et al. TGFβ signaling in the pancreatic tumor microenvironment promotes fibrosis and immune evasion to facilitate tumorigenesis. *Cancer Res*. 2016;76(9):2525–2539.
8. Kaminski N, et al. Global analysis of gene expression in pulmonary fibrosis reveals distinct programs regulating lung inflammation and fibrosis. *Proc Natl Acad Sci U S A*. 2000;97(4):1778–1783.
9. Levental KR, et al. Matrix crosslinking forces tumor progression by enhancing integrin signaling. *Cell*. 2009;139(5):891–906.
10. Cox TR, et al. LOX-mediated collagen crosslinking is responsible for fibrosis-enhanced metastasis. *Cancer Res*. 2013;73(6):1721–1732.
11. Egeblad M, Rasch MG, Weaver VM. Dynamic interplay between the collagen scaffold and tumor evolution. *Curr Opin Cell Biol*. 2010;22(5):697–706.
12. Sheppard D. Integrin-mediated activation of latent transforming growth factor β. *Cancer Metastasis Rev*. 2005;24(3):395–402.
13. Chang TT, Thakar D, Weaver VM. Force-dependent breaching of the basement membrane. *Matrix Biol*. 2017;57-58:178–189.
14. Vázquez PF, et al. TGF-β specifically enhances the metastatic attributes of murine lung adenocarcinoma: implications for human non-small cell lung cancer. *Clin Exp Metastasis*. 2013;30(8):993–1007.
15. Fernandez IE, Eickelberg O. The impact of TGF-β on lung fibrosis: from targeting to biomarkers. *Proc Am Thorac Soc*. 2012;9(3):111–116.
16. Yingling JM, Blanchard KL, Sawyer JS. Development of TGF-beta signalling inhibitors for cancer therapy. *Nat Rev Drug Discov*. 2004;3(12):1011–1022.
17. Neuzillet C, et al. Targeting the TGFβ pathway for cancer therapy. *Pharmacol Ther*. 2015;147:22–31.
18. Akhurst RJ, Hata A. Targeting the TGFβ signalling pathway in disease. *Nat Rev Drug Discov*. 2012;11(10):790–811.
19. Travis MA, Sheppard D. TGF-β activation and function in immunity. *Annu Rev Immunol*. 2014;32:51–82.
20. Mordasky Markell L, Pérez-Lorenzo R, Masiuk KE, Kennett MJ, Glick AB. Use of a TGFβ type I receptor inhibitor in mouse skin carcinogenesis reveals a dual role for TGFβ signaling in tumor promotion and progression. *Carcinogenesis*. 2010;31(12):2127–2135.
21. Lacouture ME, et al. Cutaneous keratoacanthomas/squamous cell carcinomas associated with neutralization of transforming growth factor β by the monoclonal antibody fresolimumab (GC1008). *Cancer Immunol Immunother*. 2015;64(4):437–446.
22. Anderton MJ, et al. Induction of heart valve lesions by small-molecule ALK5 inhibitors. *Toxicol Pathol*. 2011;39(6):916–924.
23. Herbertz S, et al. Clinical development of galunisertib (LY2157299 monohydrate), a small molecule inhibitor of transforming growth factor-β signaling pathway. *Drug Des Devel Ther*. 2015;9:4479–4499.
24. Blackwell TS, et al. Future directions in idiopathic pulmonary fibrosis research. An NHLBI workshop report. *Am J Respir Crit Care Med*. 2014;189(2):214–222.
25. Bandyopadhyay A, Raghavan S. Defining the role of integrin alphavbeta6 in cancer. *Curr Drug Targets*. 2009;10(7):645–652.
26. Xi Y, et al. Inhibition of epithelial-to-mesenchymal transition and pulmonary fibrosis by methacycline. *Am J Respir Cell Mol Biol*. 2014;50(1):51–60.
27. Sriram N, Kalayarasan S, Manikandan R, Arumugam M, Sudhandiran G. Epigallocatechin gallate attenuates fibroblast proliferation and excessive collagen production by effectively intervening TGF-β1 signalling. *Clin Exp Pharmacol Physiol*. 2015;42(8):849–859.
28. Wang Z, et al. Corilagin attenuates aerosol bleomycin-induced experimental lung injury. *Int J Mol Sci*. 2014;15(6):9762–9779.

29. Peng DH, et al. ZEB1 induces LOXL2-mediated collagen stabilization and deposition in the extracellular matrix to drive lung cancer invasion and metastasis. *Oncogene*. 2017;36(14):1925–1938.
30. Peinado H, et al. A molecular role for lysyl oxidase-like 2 enzyme in snail regulation and tumor progression. *EMBO J*. 2005;24(19):3446–3458.
31. Erler JT, et al. Lysyl oxidase is essential for hypoxia-induced metastasis. *Nature*. 2006;440(7088):1222–1226.
32. Sethi A, Mao W, Wordinger RJ, Clark AF. Transforming growth factor-β induces extracellular matrix protein cross-linking lysyl oxidase (LOX) genes in human trabecular meshwork cells. *Invest Ophthalmol Vis Sci*. 2011;52(8):5240–5250.
33. Finney J, Moon HJ, Ronnebaum T, Lantz M, Mure M. Human copper-dependent amine oxidases. *Arch Biochem Biophys*. 2014;546:19–32.
34. Kagan HM, Trackman PC. Properties and function of lysyl oxidase. *Am J Respir Cell Mol Biol*. 1991;5(3):206–210.
35. Yamauchi M, Sricholpech M. Lysine post-translational modifications of collagen. *Essays Biochem*. 2012;52:113–133.
36. Chen CZ, et al. The Scar-in-a-Jar: studying potential antifibrotic compounds from the epigenetic to extracellular level in a single well. *Br J Pharmacol*. 2009;158(5):1196–1209.
37. Chen CZ, Raghunath M. Focus on collagen: in vitro systems to study fibrogenesis and antifibrosis state of the art. *Fibrogenesis Tissue Repair*. 2009;2:7.
38. Hecker L, et al. NADPH oxidase-4 mediates myofibroblast activation and fibrogenic responses to lung injury. *Nat Med*. 2009;15(9):1077–1081.
39. Chen Y, et al. Lysyl hydroxylase 2 is secreted by tumor cells and can modify collagen in the extracellular space. *J Biol Chem*. 2016;291(50):25799–25808.
40. Dennler S, Itoh S, Vivien D, ten Dijke P, Huet S, Gauthier JM. Direct binding of Smad3 and Smad4 to critical TGFβ-inducible elements in the promoter of human plasminogen activator inhibitor-type 1 gene. *EMBO J*. 1998;17(11):3091–3100.
41. Raghu G, et al. Efficacy of simtuzumab versus placebo in patients with idiopathic pulmonary fibrosis: a randomised, double-blind, controlled, phase 2 trial. *Lancet Respir Med*. 2017;5(1):22–32.
42. Hornstra IK, Birge S, Starcher B, Bailey AJ, Mecham RP, Shapiro SD. Lysyl oxidase is required for vascular and diaphragmatic development in mice. *J Biol Chem*. 2003;278(16):14387–14393.
43. Mäki JM, et al. Inactivation of the lysyl oxidase gene Lox leads to aortic aneurysms, cardiovascular dysfunction, and perinatal death in mice. *Circulation*. 2002;106(19):2503–2509.
44. Mäki JM, Sormunen R, Lippo S, Kaarteenaho-Wiik R, Soininen R, Myllyharju J. Lysyl oxidase is essential for normal development and function of the respiratory system and for the integrity of elastic and collagen fibers in various tissues. *Am J Pathol*. 2005;167(4):927–936.
45. Liu X, et al. Elastic fiber homeostasis requires lysyl oxidase-like 1 protein. *Nat Genet*. 2004;36(2):178–182.
46. Peter B, Bosze S, Horvath R. Biophysical characteristics of proteins and living cells exposed to the green tea polyphenol epigallocatechin-3-gallate (EGCg): review of recent advances from molecular mechanisms to nanomedicine and clinical trials. *Eur Biophys J*. 2017;46(1):1–24.
47. Mereles D, Hunstein W. Epigallocatechin-3-gallate (EGCG) for clinical trials: more pitfalls than promises? *Int J Mol Sci*. 2011;12(9):5592–5603.
48. Zhang HM, Zhao L, Li H, Xu H, Chen WW, Tao L. Research progress on the anticarcinogenic actions and mechanisms of ellagic acid. *Cancer Biol Med*. 2014;11(2):92–100.
49. Stoner GD, et al. Pharmacokinetics of anthocyanins and ellagic acid in healthy volunteers fed freeze-dried black raspberries daily for 7 days. *J Clin Pharmacol*. 2005;45(10):1153–1164.
50. Mertens-Talcott SU, Jilma-Stohlawetz P, Rios J, Hingorani L, Derendorf H. Absorption, metabolism, and antioxidant effects of pomegranate (Punica granatum l.) polyphenols after ingestion of a standardized extract in healthy human volunteers. *J Agric Food Chem*. 2006;54(23):8956–8961.
51. Seeram NP, Henning SM, Zhang Y, Suchard M, Li Z, Heber D. Pomegranate juice ellagitannin metabolites are present in human plasma and some persist in urine for up to 48 hours. *J Nutr*. 2006;136(10):2481–2485.
52. Lee MJ, et al. Pharmacokinetics of tea catechins after ingestion of green tea and (–)-epigallocatechin-3-gallate by humans: formation of different metabolites and individual variability. *Cancer Epidemiol Biomarkers Prev*. 2002;11(10 pt 1):1025–1032.
53. Nagle DG, Ferreira D, Zhou YD. Epigallocatechin-3-gallate (EGCG): chemical and biomedical perspectives. *Phytochemistry*. 2006;67(17):1849–1855.
54. Liu J, et al. Association of green tea consumption with mortality from all-cause, cardiovascular disease and cancer in a Chinese cohort of 165,000 adult men. *Eur J Epidemiol*. 2016;31(9):853–865.
55. Lustosa BB, et al. Green tea (Cammellia sinensis) attenuates ventricular remodeling after experimental myocardial infarction. *Int J Cardiol*. 2016;225:147–153.
56. Kuriyama S, et al. Green tea consumption and mortality due to cardiovascular disease, cancer, and all causes in Japan: the Ohsaki study. *JAMA*. 2006;296(10):1255–1265.
57. Chapman HA, et al. Integrin α6β4 identifies an adult distal lung epithelial population with regenerative potential in mice. *J Clin Invest*. 2011;121(7):2855–2862.
58. Henderson NC, et al. Targeting of αv integrin identifies a core molecular pathway that regulates fibrosis in several organs. *Nat Med*. 2013;19(12):1617–1624.
59. Yamauchi M, Shiiba M. Lysine hydroxylation and cross-linking of collagen. *Methods Mol Biol*. 2008;446:95–108.